CrystEngComm

PAPER

View Article Online
View Journal | View Issue

Cite this: *CrystEngComm*, 2021, **23**, 1898

A multifunctional benzothiadiazole-based fluorescence sensor for Al^{3+}, Cr^{3+} and Fe^{3+}†

Shu-Li Yao, Yu-Chen Xiong, Xue-Mei Tian, Sui-Jun Liu,* Hui Xu, Teng-Fei Zheng,* Jing-Lin Chen and He-Rui Wen*

Received 13th January 2021,
Accepted 27th January 2021

DOI: 10.1039/d1ce00060h

rsc.li/crystengcomm

A new benzothiadiazole-based MOF $\{[Zn(BIBT)(oba)]\cdot DMA\}_n$ (**JXUST-3**, BIBT = 4,7-bi(1*H*-imidazol-1-yl) benzo-[2,1,3]thiadiazole and H_2oba = 4,4′-oxybisbenzoate) has been solvothermally synthesized and characterized by single crystal X-ray diffraction, IR spectroscopy and TGA. The fluorescence studies suggest that **JXUST-3** could simultaneously selectively sense trivalent metal ions including Al^{3+}, Cr^{3+} and Fe^{3+} by a turn-off effect, and the detection limits are 0.055, 0.049 and 0.056 μM, respectively. Moreover, **JXUST-3** exhibits relatively good thermal and chemical stabilities and reusability. The fluorescent test paper also displayed an obvious turn-off effect, indicating that **JXUST-3** can be used as a potential multi-response fluorescent probe. The possible quenching mechanisms of **JXUST-3** for Al^{3+} and Fe^{3+} were competitive energy absorption, and for Cr^{3+} ions, they were competitive energy absorption and weak interactions between Cr^{3+} and the framework. Therefore, **JXUST-3** could be viewed as a transition metal MOF fluorescence sensor for Al^{3+}, Cr^{3+} and Fe^{3+} by the turn-off effect, simultaneously.

Introduction

Metal–organic frameworks (MOFs), also known as porous coordination polymers (PCPs), are an emerging area of crystal engineering[1] and are attracting increasing attention due to their unique structures and potential applications in luminescence,[2–6] magnetism,[7,8] storage/separation,[9–12] catalysis,[13–16] ion exchange,[17] drug delivery[18] and so on. In this situation, the rational design and synthesis of MOFs are quite meaningful and a large number of such crystalline materials have been reported.[19] In recent years, with the development of industry and agriculture, environmental pollution became more serious, which is harmful to human health, especially induced by metal ions. Trivalent metal ions involving Al^{3+}, Cr^{3+}, and Fe^{3+} are some of the most serious environmental pollutants owing to their high toxicity.[20] Excessive Al^{3+} intake may cause Alzheimer's and Parkinson's disease and central nervous system dysfunction;[21] Cr^{3+} imbalance could result in diabetes and even malignant cells;[22] deficiency or overloading of Fe^{3+} in the body might lead to endotoxemia, gastrointestinal disturbance, and declining immunity.[23] Therefore, it is necessary to choose a fast and effective method to detect harmful metal ions. Due to luminescence sensing's operability and cost-saving with obvious superiorities, such as high sensitivity and selectivity, real-time response, excellent photostability and easy recognition with the naked eye, it could be considered as one of the most promising methods compared with other ways to detect metal ions.[24] Therefore, the exploration of new MOF materials with excellent fluorescence sensing ability is extremely worthy.

As is known, multitopic bridging ligands with N, S, P, and/or O-containing functional groups can exhibit diverse binding abilities for central metal ions, and therefore could be used as effective ligands for constructing various coordination networks.[19] In addition, the mixed-ligand strategy, especially the acid–base system, possesses the characteristics of compensating charge balance, coordination deficiency, repulsive vacuum, and weak interaction, simultaneously.[19] Carboxylate ligands exhibit various coordination modes and organic ligands with a richly conjugated π electron system are beneficial for preparing fluorescent MOFs with novel structures and special properties. In particular, benzothiadiazole derivatives have visible optical and electronic properties,[25,26] and are suitable to be used as an electron acceptor for molecular optoelectronic devices because of the strong electron-withdrawing capacity and high electron affinity.[27,28] To date, many MOF/CP based fluorescence sensors for Cr^{3+} and Fe^{3+}, Cr^{3+} and Al^{3+}, Al^{3+} and Fe^{3+} or $Al^{3+}/Cr^{3+}/Fe^{3+}$

School of Chemistry and Chemical Engineering, Jiangxi University of Science and Technology, Ganzhou 341000, Jiangxi Province, P.R. China.
E-mail: sjliu@jxust.edu.cn, zhengtengfei0628@163.com, wenherui63@163.com;
Tel: +86 797 8312204, +86 797 8312289

† Electronic supplementary information (ESI) available: X-ray crystallographic data file in CIF format for CCDC 2026037 (**JXUST-3**), selected bond distances and angles, SHAPE analysis of the Zn^{II} ion, IR spectrum, PXRD patterns of the simulated and experimental samples, TGA curve, CIE chromaticity diagram, luminescence decay curve, Stern–Volmer plots, XPS patterns and UV-vis absorption spectra. For ESI and crystallographic data in CIF or other electronic format see DOI: 10.1039/d1ce00060h

have been reported,[29–45] while multi-responsive fluorescence sensors for Al^{3+}, Cr^{3+} and Fe^{3+} are limited.[20,46–52] Therefore, it is still a great challenge to explore fluorescence sensors for the detection of various metal ions with multiple responses, especially the highly charged metal ions.

Herein, a new benzothiadiazole-based MOF namely $\{[Zn(BIBT)(oba)]\cdot DMA\}_n$ (**JXUST-3**) was prepared with 4,7-bi(1*H*-imidazol-1-yl)benzo-[2,1,3]thiadiazole (BIBT) and 4,4′-oxybisbenzoate (H_2oba) (Scheme 1). The fluorescence measurements demonstrated that **JXUST-3** has high sensitivity and selectivity toward Al^{3+}, Cr^{3+} and Fe^{3+} *via* a fluorescence quenching (turn-off) effect with the detection limits of 0.055, 0.049 and 0.056 μM, respectively, which are relatively low compared with those of other related fluorescence sensors.[20,46–52] Furthermore, **JXUST-3** exhibits relatively good thermal and chemical stabilities, making it a great potential fluorescence sensor for detecting Al^{3+}, Cr^{3+} and Fe^{3+}, simultaneously. Thus, **JXUST-3** could be used as a multifunctional transition metal MOF sensor for Al^{3+}, Cr^{3+} and Fe^{3+} through the turn-off effect.

Experimental section

Materials and instrumentation

The BIBT ligand was obtained through the way reported by our group,[53] and other chemicals were analytical grade, purchased from commercial sources and used without purification. The powder X-ray diffraction (PXRD) spectra were measured on a Rigaku MiniFlex 600 instrument. The simulated PXRD spectrum was obtained from the single-crystal data from Mercury (Hg) program, which is freely available on the internet at http://www.iucr.org. The IR spectrum was recorded on a Bruker ALPHA FT-IR spectrometer with KBr pellets in the range of 4000–400 cm^{-1}. Thermogravimetric analysis (TGA) was carried out using a NETZSCH STA2500 (TG/DTA) under an N_2 atmosphere from room temperature to 800 °C. The fluorescence emission spectra of the solid and liquid were recorded on a Hitachi F4600 fluorescence spectrophotometer. The luminescence lifetime was measured on a HORIBA Flourolog fluorescence spectrophotometer. The UV-vis absorption spectra were collected on a UV-2550 spectrophotometer.

Synthesis of $\{[Zn(BIBT)(oba)]\cdot DMA\}_n$ (JXUST-3)

$Zn(NO_3)_2\cdot 6H_2O$ (15.0 mg, 0.05 mmol), H_2oba (12.9 mg, 0.05 mmol) and BIBT (13.4 mg, 0.05 mmol) were dissolved in the mixed solvent of 3 mL DMA, 0.25 mL EtOH and 0.25 mL H_2O in a 25 mL Teflon-lined autoclave. After the mixture was sonicated for 10 minutes, the autoclave was sealed and placed in a 120 °C oven for 3 days. Yellow block crystals were gained after the autoclave cooling to room temperature for 24 h. The yield was about 25% based on Zn^{II}. IR spectrum (cm^{-1}): 3832m, 3731m, 3666m, 3443m, 3140w, 2926w, 1602s, 1522s, 1382s, 1317w, 1236s, 1160m, 1085m, 1019w, 944w, 876m, 779w, 698w, 654m, 513w, 434w (Fig. S1, ESI†).

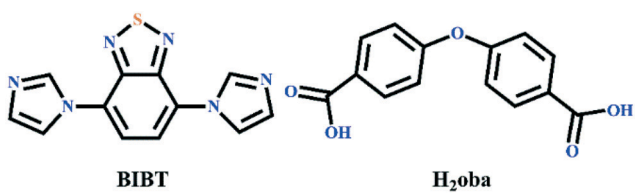

Scheme 1 BIBT and H_2oba ligands used for the synthesis of **JXUST-3**.

Crystallographic studies for JXUST-3

The single-crystal X-ray diffraction data for **JXUST-3** were collected on a Bruker D8 QUEST diffractometer with Mo-Kα radiation (λ = 0.71073 Å) in ω scan mode. SAINT program was applied to integrate the diffraction profiles.[54] The structure was processed by the direct method and refined by the full-matrix least squares methods with SHELX 2017/1.[55,56] The non-hydrogen atoms were situated in successive difference Fourier syntheses and refined by anisotropic thermal parameters on F^2. The hydrogen atoms of the BIBT and H_2oba ligands were theoretically generated at the specific atoms and refined isotropically by fixed thermal factors. The summary of the crystallographic data and refinement parameters of **JXUST-3** is shown in Table 1. The selected bond distances and angles of **JXUST-3** are displayed in Table S1 (ESI†).

Results and discussion

Synthesis

JXUST-3 was constructed with the mixed ligands H_2oba and BIBT with $Zn(NO_3)_2\cdot 6H_2O$ in the solvents DMA, EtOH and H_2O at 120 °C. The IR spectrum shows that there are peaks with strong intensity at 1602 cm^{-1} and 1382 cm^{-1}, which are

Table 1 Crystal data and structure refinements of **JXUST-3**

Compound	**JXUST-3**
Formula	$C_{30}H_{25}N_7O_6SZn$
*M*r	677.00
T (K)	273(2)
Crystal system	Triclinic
Space group	$P\bar{1}$
a (Å)	11.1974(3)
b (Å)	12.7343(3)
c (Å)	12.9086(3)
α (°)	64.468(1)
β (°)	73.240(1)
γ (°)	64.474(1)
V (Å^3)	1486.83(7)
Z	2
F(000)	696
D_{calc} (g cm^{-3})	1.512
μ (mm^{-1})	0.95
Reflections collected/unique	22 594/6773
R_{int}	0.026
$R_1{}^a/wR_2{}^b$ [$I > 2\sigma(I)$]	0.0405/0.0945
$R_1{}^a/wR_2{}^b$ (all data)	0.0553/0.1034
GOF on F^2	1.02

^{a} $R_1 = \sum(||F_o| - |F_C||)/\sum|F_o|$. ^{b} $wR_2 = [\sum w(|F_o|^2 - |F_C|^2)^2/(\sum w|F_o|^2)^2]^{1/2}$.

possibly related to –COO^- groups. The peaks at 1522 cm^{-1} and 1317 cm^{-1} may be attributed to imidazole ring stretching.

Structural characterization

Single-crystal X-ray diffraction results show that **JXUST-3** crystallizes in the triclinic $P\bar{1}$ space group. The asymmetric unit of **JXUST-3** includes one Zn^{II} ion, one BIBT ligand, one oba^{2-} anion and one DMA molecule (Fig. 1a). Each Zn^{II} ion is six-coordinated, and is composed of four oxygen atoms (O1, O2, O4B and O5B) from two oba^{2-} anions and two nitrogen atoms (N1 and N6A) from two BIBT ligands. The Zn–O and Zn–N bond distances are in the ranges of 2.117(2)–2.313(2) Å and 2.0552(19)–2.0699(19) Å, respectively (Table S1, ESI†). The Zn1 coordination geometry could be regarded as an octahedron, which was calculated by the SHAPE 2.1 software[57] (Table S2, ESI†). The adjacent Zn^{II} ions are linked by BIBT to obtain Zn^{II}-BIBT chains, and then the chains are further connected by oba^{2-} to form a two-dimensional (2D) sheet layer structure (Fig. 1b). From the topological analysis, if each Zn^{II} ion is viewed as a 4-connected node, the whole 2D structure of **JXUST-3** could be simplified as a (4,4) sheet. Then, the 2D layers are further packed by π–π interaction to gain a three-dimensional (3D) supramolecular architecture (Fig. 1c). The porosity is 25.3% and the total solvent-accessible volume is 376.4 $Å^3$, which is estimated by PLATON.[58]

PXRD patterns and TGA

The PXRD patterns were recorded to verify the phase purity, cycle stability and solvent stability of **JXUST-3**. The PXRD pattern of the as-synthesized sample fits well with the simulated one, implying that the experimental sample is pure phase (Fig. S2a, ESI†). Moreover, the samples were also soaked in some common organic solvents, including *N*,*N*-dimethylformamide (DMF), dimethylacetamide (DMA), *n*-hexane, acetonitrile (CH_3CN), acetone, tetrahydrofuran (THF), H_2O, and dichloromethane (CH_2Cl_2) for 24 h, and the PXRD patterns of the experimental samples are also consistent with the simulated one (Fig. S2b, ESI†), which elucidates that **JXUST-3** has relatively good solvent stability.

In addition, the thermal stability of **JXUST-3** was measured by TGA measurement. The result shows that **JXUST-3** has weight loss from room temperature to 245 °C, which could be due to the removal of the crystal surface and channel solvent molecules (weight loss obsd: 13.71%, calcd: 12.87% (one DMA molecule)). Hereafter, the framework begins to collapse at above 370 °C, demonstrating that **JXUST-3** could be stable below 370 °C and displays relatively good thermal stability (Fig. S3, ESI†).

Fluorescence behaviors

JXUST-3 is constructed from d^{10} metal ion Zn^{II} and organic fluorescent ligands, and could be deemed as a promising fluorescent material.[59] The solid fluorescence emission spectra of BIBT and **JXUST-3** were measured at room temperature. As displayed in Fig. 2, the emission bands are observed at 527 nm (λ_{ex} = 466 nm) for BIBT and 492 nm (λ_{ex} = 286 nm) for **JXUST-3**, respectively. In addition, the fluorescence emission of **JXUST-3** is consistent with the CIE chromaticity diagram (Fig. S4, ESI†). The emission band of H_2oba is at 317 nm (λ_{ex} = 276 nm).[60] As is known, a double bond composed of σ and π bonds and the emission of the organic ligands are usually ascribed to π* → π and/or π* → n electronic transitions.[61] Therefore, the fluorescence emission of **JXUST-3** should be largely on account of the metal-perturbed intraligand charge transfer owing to the d^{10} electron configuration of Zn^{II}. Furthermore, the obvious blue-shift of the emission band compared with that of the BIBT ligand may be due to the metal–ligand coordination interactions.[59,62] In addition, different coordination environments also have an important influence on the emission of **JXUST-3**.[59] Moreover, the fluorescence decay curve indicates that the fluorescence lifetime of **JXUST-3** is 4.42 μs (Fig. S5, ESI†).

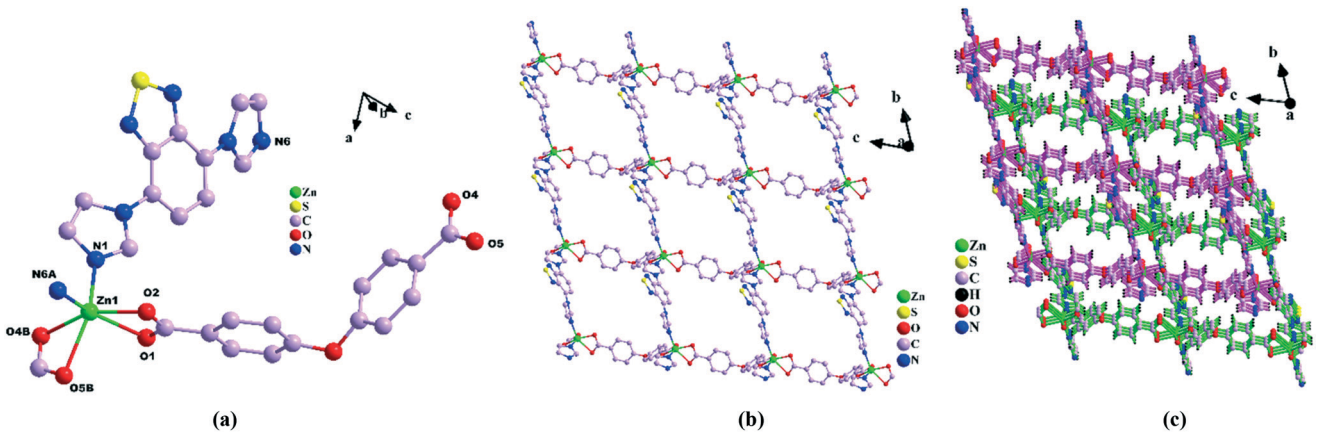

Fig. 1 Views of (a) the coordination environment of the Zn^{II} ion in **JXUST-3** (H atoms omitted for clarity), symmetry codes: A: $x + 1, y - 1, z$; B: $x + 1, y, z - 1$; (b) the 2D structure of **JXUST-3**; (c) the 3D supramolecular architecture of **JXUST-3**.

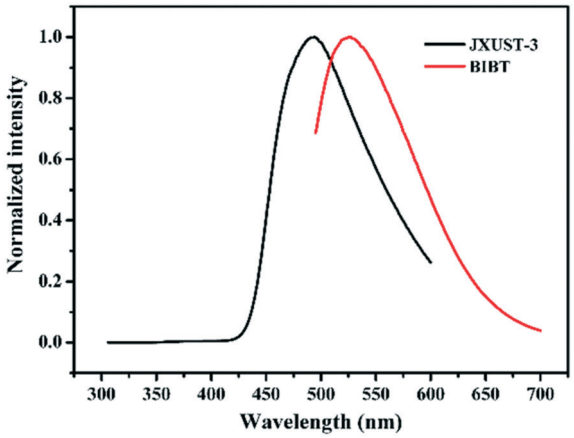

Fig. 2 The solid fluorescence emission spectra for BIBT and **JXUST-3**.

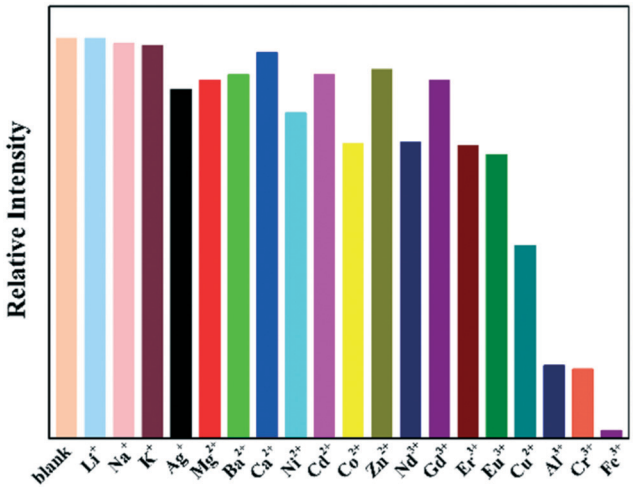

Fig. 3 Fluorescence relative intensities of **JXUST-3** in an EtOH suspension with different metal ions (0.3 mM), λ_{ex} = 286 nm.

Metal-ion detection

The fluorescence detection experiments of various metal ions were carried out in an EtOH suspension at room temperature. Because **JXUST-3** was constructed in EtOH solution and with environmentally friendly characteristics, EtOH was chosen as the dispersion medium. The **JXUST-3** samples were fully milled and immersed in EtOH solution with the rate of 1 mg per 2 mL, and then the mixture was ultrasonically treated for half an hour to obtain a stable suspension. In order to explore the fluorescence sensing behavior of **JXUST-3** toward metal ions, 6 μL 0.1 mol L^{-1} different metal ion solutions were added in a 2 mL EtOH suspension in a 3 mL quartz cuvette ($M(NO_3)_x$; M = Na^+, Li^+, Ag^+, K^+, Mg^{2+}, Ba^{2+}, Ca^{2+}, Ni^{2+}, Co^{2+}, Cd^{2+}, Zn^{2+}, Cu^{2+}, Nd^{3+}, Eu^{3+}, Gd^{3+}, Er^{3+}, Al^{3+}, Cr^{3+} and Fe^{3+}; x = 1, 2 and 3; the test concentration is 0.3 mM). As illustrated in Fig. 3, after the addition of different metal ions, most of them had a relatively weak effect on the fluorescence emission intensity of **JXUST-3**, while Al^{3+}, Cr^{3+} and Fe^{3+} ions displayed a relatively obvious fluorescence quenching effect, especially Fe^{3+} ions showing a nearly complete quenching effect. The results demonstrate that **JXUST-3** has good selectivity toward Al^{3+}, Cr^{3+} and Fe^{3+} ions.

Moreover, the anti-interference experiments of Al^{3+}, Cr^{3+} and Fe^{3+} were also performed (Fig. 4a, c and e). 1 equiv. of Al^{3+}/Cr^{3+}/Fe^{3+} metal ions was added to the other metal ion suspensions, and the fluorescence quenching effect still existed, revealing the excellent sensitivity characteristic of **JXUST-3** toward Al^{3+}, Cr^{3+} and Fe^{3+} ions. To investigate the correlation between the concentration and emission intensity, the fluorescence titration experiments were carried out with the increasing concentrations of Al^{3+}/Cr^{3+}/Fe^{3+} ions, and the fluorescence intensities gradually decreased with the addition of Al^{3+}/Cr^{3+}/Fe^{3+} ions. The correlation between the fluorescence emission intensity ratios I_0/I and the concentrations of Al^{3+}/Cr^{3+}/Fe^{3+} is exhibited in Fig. S6 (ESI†), which shows a good linear correlation (R^2 = 0.994, 0.995 and 0.994). And the detection limits were 0.055, 0.049 and 0.056 μM, respectively, which were calculated by $3\sigma/k$ (σ: the standard error; k: the slope). Although several MOF-based materials display fluorescence sensing toward Al^{3+}, Cr^{3+} and Fe^{3+} ions, **JXUST-3** has relatively low detection limits by the turn-off effect (Table 2).[20,46–52] These results demonstrate that **JXUST-3** could be viewed as a multifunctional fluorescent probe for Al^{3+}, Cr^{3+} and Fe^{3+} with high sensitivity and selectivity.

In addition, fluorescent test paper was prepared for practical application by immersing the filter paper in the EtOH suspension of **JXUST-3**. Then, the capillaries were used to absorb Fe^{3+}/Al^{3+}/Cr^{3+} ions solution to write the corresponding element symbols. The results demonstrate that there is a fluorescence quenching effect with different quenching degrees (Fig. 5). Therefore, the fluorescent test paper provides a facile, fast, portable and naked-eye recognizable method under UV light for the selective detection of Al^{3+}, Cr^{3+} and Fe^{3+} ions.

Recycling capability is also an important indicator in practical applications. Thus, a fast and simple method to evaluate the recycling capability of **JXUST-3** for the fluorescence sensing of Al^{3+}, Cr^{3+} and Fe^{3+} is carried out. The as-synthesized sample of **JXUST-3** was simply immersed in 0.3 mM Al^{3+}/Cr^{3+}/Fe^{3+} ion EtOH solution for fifteen minutes and then washed five times with EtOH, respectively. As displayed in Fig. 6, the fluorescence intensities show a slight change and the PXRD patterns of the recycled samples are well consistent with the simulated one (Fig. S2c, ESI†), revealing that the framework is still stable. Therefore, **JXUST-3** can be cyclically utilized at least four times as a multifunctional fluorescence sensor for Al^{3+}, Cr^{3+} and Fe^{3+} ions.

To investigate the possible turn-off sensing mechanism toward Al^{3+}, Cr^{3+} and Fe^{3+}, the related experiments were carried out. As we know, the fluorescence quenching mechanisms may be due to reasons including the collapse of the structure, exchange of cations, energy competition of absorption and interactions between sensing ions and MOF frameworks.[20,47] The PXRD patterns of **JXUST-3** immersed in Al^{3+}, Cr^{3+} and Fe^{3+} ions are consistent with the simulated

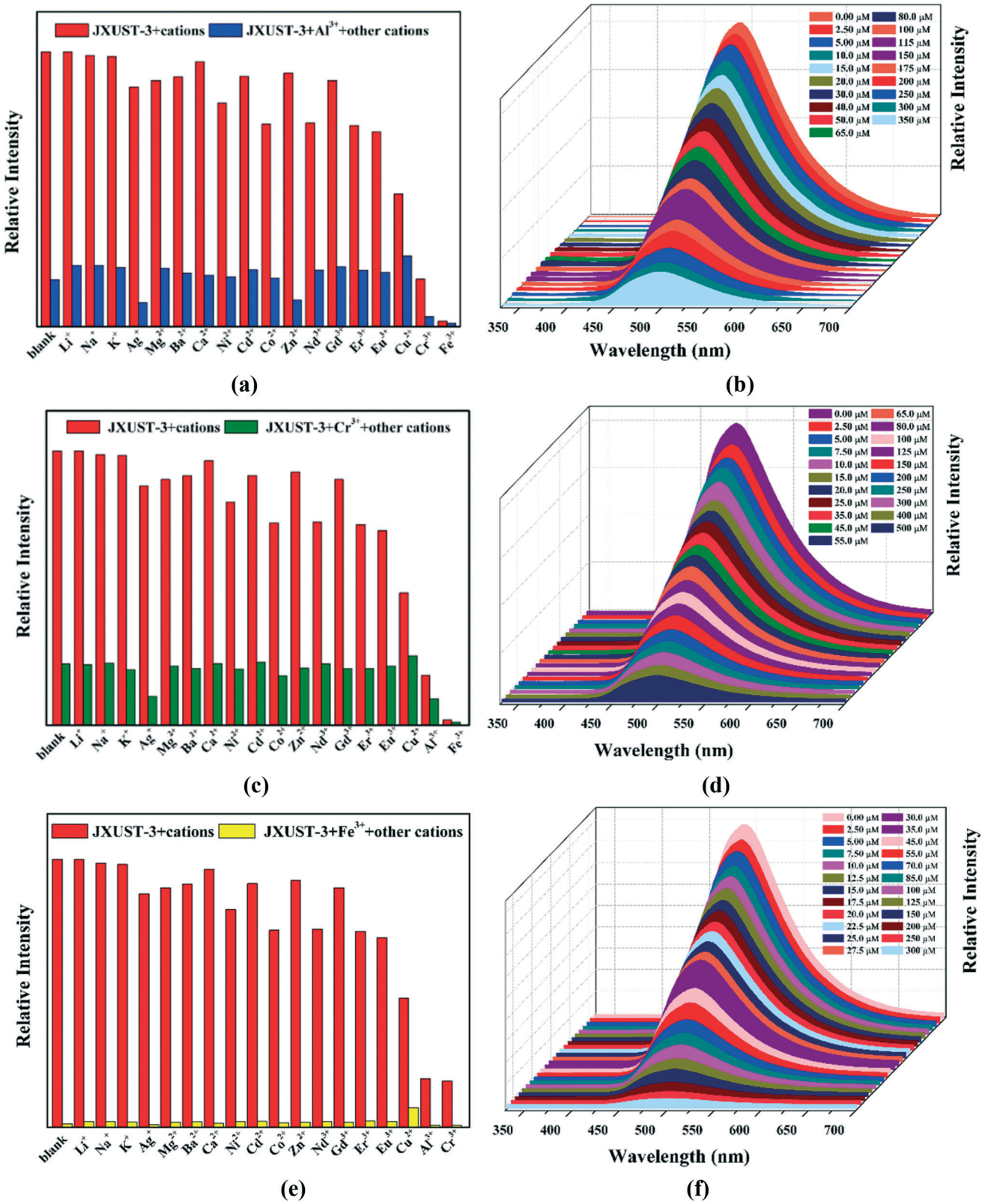

Fig. 4 Fluorescence intensity ratio histograms of **JXUST-3** dispersed in EtOH with different metal ions (red) and subsequent addition of 1 equiv. of Al^{3+} ions (blue) (a), Cr^{3+} ions (green) (c) and Fe^{3+} ions (yellow) (e) and the fluorescence intensities of **JXUST-3** in the different concentrations of Al^{3+} ions (b), Cr^{3+} ions (d) and Fe^{3+} ions (f), respectively.

Table 2 The summary of the detection limits for detecting Al^{3+}, Cr^{3+} and Fe^{3+} simultaneously

Complex	Detection limit of Al^{3+}	Detection limit of Cr^{3+}	Detection limit of Fe^{3+}	Medium solvent	Ref.
{[Zn(BIBT)(oba)]·DMA}$_n$ (**JXUST-3**)	0.055 μM (off)	0.049 μM (off)	0.056 μM (off)	EtOH	This work
Tb–TCPP	7.79 nM (on)	9.94 nM (on)	16.4 nM (on)	DMF	52
[Zn(5-NH_2-1,3-bdc)(H_2O)]	2.44 μM (off–on)	13.9 μM (off–on)	0.317 μM (off)	H_2O	51
[Zn_2(5-NH_2-1,3-bdc)$_2$(NI-bpy-44)]·DMF	5.59 μM (off)	7.87 μM (off)	0.709 μM (off)	H_2O	51
[Eu(DLDA)(DMF)(H_2O)(COO)]$_n$	2.38 μM (off)	0.945 μM (off)	1.93 μM (off)	DMA	46
[Eu_2(ppda)$_2$(npdc)(H_2O)]·H_2O	0.011 μM (off)	0.617 μM (off)	0.166 μM (off)	H_2O	47
{[Co_3(BIBT)$_3$(BTC)$_2$(H_2O)$_2$]·solvents}$_n$ (**JXUST-2**)	0.10 μM (on)	0.10 μM (on)	0.13 μM (on)	DMA	48
[Cd(Hcip)(bpea)$_{0.5}$(H_2O)]$_n$	1.31 μM (on)	1.84 μM (on)	3.24 μM (off)	DMF	20
{[Tb_2(HL)$_2$(H_2O)$_4$]·2Cl·5H_2O}$_n$	— (off)	— (off)	— (off)	H_2O	49
{[Zn_4(DPBT)$_2$(BDC)$_4$]·H_2O·2DPBT}$_n$	— (on)	— (on)	— (off)	DMF	50

Fig. 5 The fluorescent test paper treated with Al^{3+}, Cr^{3+} and Fe^{3+} ions (0.1 M).

one, confirming the structural stability of **JXUST-3**. Thus, the fluorescence quenching effects of the Al^{3+}, Cr^{3+} and Fe^{3+} ions were not caused by the framework collapse (Fig. S2a, ESI†). In addition, owing to the neutral framework and difference of electron configuration, it is very difficult for **JXUST-3** to achieve the turn-off effect by the exchange of the Al^{3+}/Cr^{3+}/Fe^{3+} ions with the central Zn^{2+} within the framework. Furthermore, the XPS spectra of **JXUST-3**@Al^{3+}/Cr^{3+}/Fe^{3+} (the **JXUST-3** sample immersed in 0.3 mM Al^{3+}/Cr^{3+}/Fe^{3+} and washed with EtOH five times) displayed that there was a Cr 2p peak after the sample immersion in Cr^{3+} ions, while there are no obvious peaks of Al 2p and Fe 2p after the sample immersion in Al^{3+} and Fe^{3+} ions[63–65] (Fig. S7, ESI†), indicating that Cr^{3+} ions may exist in the framework and induce interactions with **JXUST-3**.[36,52] Importantly, the UV-vis absorption spectra of the Al^{3+}, Cr^{3+} and Fe^{3+} ions show that there are overlaps with the excitation spectrum of **JXUST-3** (Fig. S8, ESI†). Therefore, the excitation energy may be absorbed by the Al^{3+}, Cr^{3+} and Fe^{3+} ions. Consequently, the possible luminescence quenching mechanism for the Al^{3+} and Fe^{3+} ions may be owing to the energy competitive absorption, and for the Cr^{3+} ions, it may be due to the competitive energy absorption and weak interactions between Cr^{3+} and the framework of **JXUST-3**.

Conclusions

In conclusion, a new benzothiadiazole-based MOF (**JXUST-3**) was synthesized by a mixed-ligand strategy with BIBT and H_2oba under solvothermal conditions. **JXUST-3** displays relatively good thermal and chemical stability. Interestingly, fluorescence detection experiments demonstrated that **JXUST-3** could simultaneously selectively probe trivalent Al^{3+}, Cr^{3+} and Fe^{3+} ions *via* a turn-off effect with relatively high selectivity and sensitivity, anti-interference ability and recycling performance. The detection limits are 0.055, 0.049 and 0.056 μM, respectively. In addition, **JXUST-3** was also manufactured as a fluorescent test paper for practical applications, and the test paper also displayed the obvious turn-off effect. Importantly, **JXUST-3** could be considered as a transition metal MOF based fluorescence sensor for Al^{3+}, Cr^{3+} and

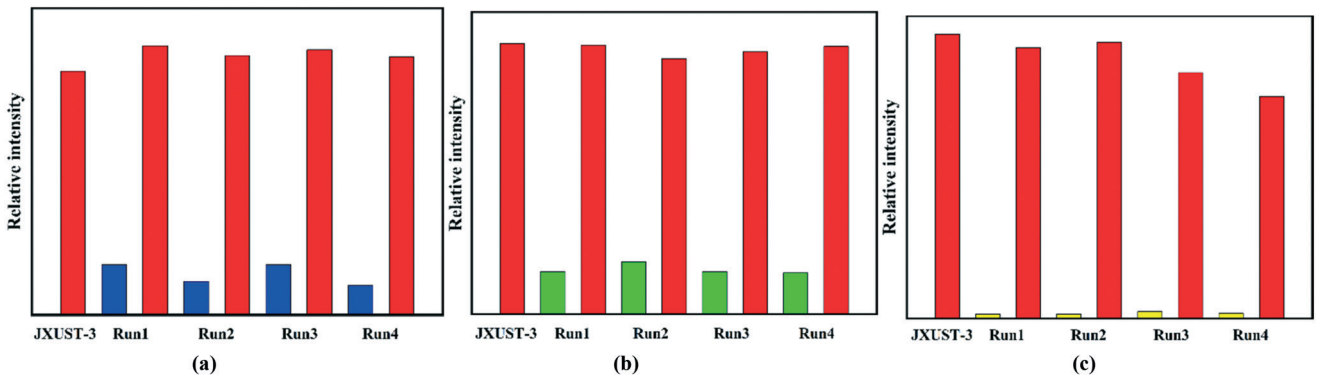

Fig. 6 The fluorescence relative intensities of **JXUST-3** after four times of recycling toward Al^{3+} ions (a), Cr^{3+} ions (b) and Fe^{3+} ions (c) (λ_{ex} = 286 nm).

Fe^{3+} by turn-off effects. Furthermore, the possible fluorescence quenching mechanisms of **JXUST-3** for Al^{3+} and Fe^{3+} were energy competitive absorption, and for Cr^{3+} ions, they were energy competitive absorption and weak interactions between Cr^{3+} and **JXUST-3**. Therefore, **JXUST-3** could be viewed as a potential multifunctional fluorescence sensor for Al^{3+}, Cr^{3+} and Fe^{3+}. Further studies of BIBT-based fluorescent MOF materials are ongoing in our laboratory.

Conflicts of interest

There are no conflicts to declare.

Acknowledgements

This work was supported by the National Natural Science Foundation of China (22061019, 21761012, and 21861018), the Natural Science Foundation of Jiangxi Province of China (20192BAB203001, 20202ACBL213001, 20192ACBL20013, and 20182BCB22010), the Youth Jinggang Scholars Program in Jiangxi Province and Special Foundation for Postgraduate Innovation in Jiangxi Province (YC2020-B155).

References

1 Z. Chang, D. H. Yang, J. Xu, T. L. Hu and X. H. Bu, *Adv. Mater.*, 2015, **27**, 5432–5441.
2 R. Goswami, S. C. Mandal, B. Pathak and S. Neogi, *ACS Appl. Mater. Interfaces*, 2019, **11**, 9042–9053.
3 D. Gu, W. Yang, G. Ning, F. Wang, S. Wu, X. Shi, Y. Wang and Q. Pan, *Inorg. Chem.*, 2020, **59**, 1778–1784.
4 S. L. Yao, S. J. Liu, X. M. Tian, T. F. Zheng, C. Cao, C. Y. Niu, Y. Q. Chen, J. L. Chen, H. Huang and H. R. Wen, *Inorg. Chem.*, 2019, **58**, 3578–3581.
5 G. X. Wen, M. L. Han, X. Q. Wu, Y. P. Wu, W. W. Dong, J. Zhao, D. S. Li and L. F. Ma, *Dalton Trans.*, 2016, **45**, 15492–15499.
6 W. Huang, G. B. Hu, L. Y. Yao, Y. Yang, W. B. Liang, R. Yuan and D. R. Xiao, *Anal. Chem.*, 2020, **92**, 3380–3387.
7 E. Coronado and G. M. Espallargas, *Chem. Soc. Rev.*, 2013, **42**, 1525–1539.
8 S. J. Liu, C. Cao, S. L. Yao, T. F. Zheng, Z. X. Wang, C. Liu, J. S. Liao, J. L. Chen, Y. W. Li and H. R. Wen, *Dalton Trans.*, 2016, **46**, 64–70.
9 H. Li, K. Wang, Y. Sun, C. T. Lollar, J. Li and H. C. Zhou, *Mater. Today*, 2018, **21**, 108–121.
10 R. B. Lin, H. Wu, L. Li, X. L. Tang, Z. Li, J. Gao, H. Cui, W. Zhou and B. Chen, *J. Am. Chem. Soc.*, 2018, **140**, 12940–12946.
11 Y. W. Li, H. Yan, T. L. Hu, H. Y. Ma, D. C. Li, S. N. Wang, Q. X. Yao, J. M. Dou, J. Xu and X. H. Bu, *Chem. Commun.*, 2017, **53**, 2394–2397.
12 Y. W. Li, J. Xu, D. C. Li, J. M. Dou, H. Yan, T. L. Hu and X. H. Bu, *Chem. Commun.*, 2015, **51**, 14211–14214.
13 D. Yang and B. C. Gates, *ACS Catal.*, 2019, **9**, 1779–1798.
14 J. D. Xiao and H. L. Jiang, *Acc. Chem. Res.*, 2019, **52**, 356–366.
15 Y. W. Li, W. J. Zhang, J. Li, H. Y. Ma, H. M. Du, D. C. Li, S. N. Wang, J. S. Zhao, J. M. Dou and L. Xu, *ACS Appl. Mater. Interfaces*, 2020, **12**, 44710–44719.
16 H. Hu, D. Zhang, H. Liu, Y. Jin, J. Gao, Y. Zhang, Z. Liu, X. Zhang, L. Geng, S. Liu and R. Zhang, *Chin. Chem. Lett.*, 2021, DOI: 10.1016/j.cclet.2020.02.028.
17 P. Kumar, A. Pournara, K. H. Kim, V. Bansal, S. Rapti and M. J. Manos, *Prog. Mater. Sci.*, 2017, **86**, 25–74.
18 W. Cai, J. Wang, C. Chu, W. Chen, C. Wu and G. Liu, *Adv. Sci.*, 2019, **6**, 1801526.
19 M. Du, C. P. Li, C. S. Liu and S. M. Fang, *Coord. Chem. Rev.*, 2013, **257**, 1282–1305.
20 Y. Yu, Y. Wang, H. Yan, J. Lu, H. Liu, Y. Li, S. Wang, D. Li, J. Dou, L. Yang and Z. Zhou, *Inorg. Chem.*, 2020, **59**, 3828–3837.
21 B. Wang, W. Xing, Y. Zhao and X. Deng, *Environ. Toxicol. Pharmacol.*, 2010, **29**, 308–313.
22 R. Lv, J. Wang, Y. Zhang, H. Li, L. Yang, S. Liao, W. Gu and X. Liu, *J. Mater. Chem. A*, 2016, **4**, 15494–15500.
23 M. Zheng, H. Tan, Z. Xie, L. Zhang, X. Jing and Z. Sun, *ACS Appl. Mater. Interfaces*, 2013, **5**, 1078–1083.
24 M. Wang, L. Guo and D. Cao, *Sens. Actuators, B*, 2018, **256**, 839–845.
25 W. Q. Zhang, K. Cheng, H. Zhang, Q. Y. Li, Z. Ma, Z. Wang, J. Sheng, Y. Li, X. Zhao and X. J. Wang, *Inorg. Chem.*, 2018, **57**, 4230–4233.
26 W. Q. Zhang, Q. Y. Li, J. Y. Cheng, K. Cheng, X. Yang, Y. Li, X. Zhao and X. J. Wang, *ACS Appl. Mater. Interfaces*, 2017, **9**, 31352–31356.
27 X. Han, W. Gong, Y. Tong, D. Wei, Y. Wang, J. Ding, H. Hou and Y. Song, *Dyes Pigm.*, 2017, **137**, 135–142.
28 X. Han, Z. Wang, Q. Cheng, X. Meng, D. Wei, Y. Zheng, J. Ding and H. Hou, *Dyes Pigm.*, 2017, **145**, 576–583.
29 H. Wang, J. Qin, C. Huang, Y. Han, W. Xu and H. Hou, *Dalton Trans.*, 2016, **45**, 12710–12716.
30 Y. Liu, C. Liu, X. Zhang, L. Liu, C. Ge, X. Zhuang, N. Zhang, Q. Yang, Y. Q. Huang and Z. Zhang, *J. Solid State Chem.*, 2019, **272**, 1–8.
31 L. H. Cao, F. Shi, W. M. Zhang, S. Q. Zang and T. C. Mak, *Chem*, 2015, **21**, 15705–15712.
32 D. M. Chen, N. N. Zhang, C. S. Liu and M. Du, *J. Mater. Chem. C*, 2017, **5**, 2311–2317.
33 Z. Chen, Y. Sun, L. Zhang, D. Sun, F. Liu, Q. Meng, R. Wang and D. Sun, *Chem. Commun.*, 2013, **49**, 11557–11559.
34 B. B. Kang, N. Wei and Z. B. Han, *RSC Adv.*, 2015, **5**, 1605–1611.
35 Y. Dai, J. J. Zhang, S. Q. Liu, H. Zhou, Y. J. Sun, Y. Z. Pan, J. Ni and J. S. Yang, *Chem*, 2018, **24**, 9555–9564.
36 M. H. Yu, T. L. Hu and X. H. Bu, *Inorg. Chem. Front.*, 2017, **4**, 256–260.
37 D. K. Singha and P. Mahata, *Inorg. Chem.*, 2015, **54**, 6373–6379.
38 W. M. Chen, X. L. Meng, G. L. Zhuang, Z. Wang, M. Kurmoo, Q. Q. Zhao, X. P. Wang, B. Shan, C. H. Tung and D. Sun, *J. Mater. Chem. A*, 2017, **5**, 13079–13085.
39 J. N. Hao and B. Yan, *J. Mater. Chem. C*, 2014, **2**, 6758–6764.

40 S. R. Zhang, J. Li, D. Y. Du, J. S. Qin, S. L. Li, W. W. He, Z. M. Su and Y. Q. Lan, *J. Mater. Chem. A*, 2015, **3**, 23426–23434.
41 X. X. Jia, R. X. Yao, F. Q. Zhang and X. M. Zhang, *Inorg. Chem.*, 2017, **56**, 2690–2696.
42 X. Y. Guo, F. Zhao, J. J. Liu, Z. L. Liu and Y. Q. Wang, *J. Mater. Chem. A*, 2017, **5**, 20035–20043.
43 Z. Chen, X. Mi, J. Lu, S. Wang, Y. Li, J. Dou and D. Li, *Dalton Trans.*, 2018, **47**, 6240–6249.
44 X. Mi, D. Sheng, Y. Yu, Y. Wang, L. Zhao, J. Lu, Y. Li, D. Li, J. Dou, J. Duan and S. Wang, *ACS Appl. Mater. Interfaces*, 2019, **11**, 7914–7926.
45 Y. W. Li, J. Li, X. Y. Wan, D. F. Sheng, H. Yan, S. S. Zhang, H. Y. Ma, S. N. Wang, D. C. Li, Z. Y. Gao, J. M. Dou and D. Sun, *Inorg. Chem.*, 2021, **60**, 671–681.
46 B. Li, J. Zhou, F. Bai and Y. Xing, *Dyes Pigm.*, 2020, **172**, 107862.
47 Z. Zhan, X. Liang, X. Zhang, Y. Jia and M. Hu, *Dalton Trans.*, 2019, **48**, 1786–1794.
48 X. M. Tian, S. L. Yao, C. Q. Qiu, T. F. Zheng, Y. Q. Chen, H. Huang, J. L. Chen, S. J. Liu and H. R. Wen, *Inorg. Chem.*, 2020, **59**, 2803–2810.
49 W. Wang, R. Wang, Y. Ge and B. Wu, *RSC Adv.*, 2018, **8**, 42100–42108.
50 K. Shen, Z. Ju, L. Qin, T. Wang and H. Zheng, *Dyes Pigm.*, 2017, **136**, 515–521.
51 J. R. Zhang, J. J. Lee, C. H. Su, M. J. Tsai, C. Y. Li and J. Y. Wu, *Dalton Trans.*, 2020, **49**, 14201–14215.
52 C. Fu, X. Sun, G. Zhang, P. Shi and P. Cui, *Inorg. Chem.*, 2021, **60**, 1116–1123.
53 X. M. Tian, S. L. Yao, J. Wu, H. Xie, T. F. Zheng, X. J. Jiang, Y. Wu, J. Mao and S. J. Liu, *Polyhedron*, 2019, **171**, 523–529.
54 *SAINT, Version 6.02a*, Bruker AXS Inc, Madison, WI, 2002.
55 G. M. Sheldrick, *Acta Crystallogr., Sect. A: Found. Adv.*, 2015, **71**, 3–8.
56 G. M. Sheldrick, *Acta Crystallogr., Sect. C: Struct. Chem.*, 2015, **71**, 3–8.
57 M. Llunell, D. Casanova, J. Cirera, P. Alemany and S. Alvarez, *SHAPE, version 2.1*, Universitat de Barcelona, Barcelona, Spain, 2013.
58 A. L. Spek, *Acta Crystallogr., Sect. C: Struct. Chem.*, 2015, **71**, 9–18.
59 D. Zhao, X. H. Liu, Y. Zhao, P. Wang, Y. Liu, M. Azam, S. I. Al-Resayes, Y. Lu and W. Y. Sun, *J. Mater. Chem. A*, 2017, **5**, 15797–15807.
60 S. Tripathi, S. K. Sachan and G. Anantharaman, *Polyhedron*, 2016, **119**, 55–70.
61 Y. Wang, P. Xu, Q. Xie, Q. Q. Ma, Y. H. Meng, Z. W. Wang, S. Zhang, X. J. Zhao, J. Chen and Z. L. Wang, *Chem. – Eur. J.*, 2016, **22**, 10459–10474.
62 X. G. Guo, W. B. Yang, X. Y. Wu, Q. K. Zhang, L. Lin, R. M. Yu and C. Z. Lu, *CrystEngComm*, 2013, **15**, 3654–3663.
63 S. G. Menon, A. K. Kunti, S. D. Kulkarni, R. Kumar, M. Jain, D. Poelman, J. J. Joos and H. C. Swart, *J. Lumin.*, 2020, **226**, 117482.
64 M. Niu, G. Li, L. Cao, X. Wang and W. Wang, *J. Cleaner Prod.*, 2020, **256**, 120700.
65 A. A. Aryee, F. M. Mpatani, X. Zhang, A. N. Kani, E. Dovi, R. Han, Z. Li and L. Qu, *J. Cleaner Prod.*, 2020, **268**, 122191.